Metal-insulator transition in an one-dimensional two-band Hubbard-like model

1995 J. Phys.: Condens. Matter 7 111

(http://iopscience.iop.org/0953-8984/7/1/011)

J. Phys.: Condens. Matter 7 (1995) 111–132. Printed in the UK

Metal–insulator transition in an one-dimensional two-band Hubbard-like model

P Schlottmann

Department of Physics, Florida State University, Tallahassee, FL 32306, USA

Received 22 July 1994, in final form 13 September 1994

Abstract. We consider a one-dimensional two-band model of electrons on a lattice with equal nearest-neighbour hopping, an interband splitting Δ and a Hubbard-like repulsion U. The model is defined via the SU(4) generalization of Lieb and Wu's Bethe *ansatz* solution of the one-dimensional Hubbard model. At $T = 0$ the model has a Mott metal–insulator transition at a critical value $U_c(\Delta)$ for a band filling of exactly one electron per site. U_c decreases with Δ, being zero if the excited-electron band is empty, and $U_c = 2.981$ when the bands are degenerate. We discuss the ground-state properties, the spectrum of elemental excitations, the specific heat and the magnetic susceptibility, in both the metallic and insulating phases, as a function of the crystal-field splitting for exactly one electron per site. There are four branches of elemental excitations: (i) charge excitations, (ii) crystalline-field excitations and (iii) two branches of spin waves. The Fermi velocity is finite in the metallic phase, diverges as the metal–insulator transition is approached from the metallic side and vanishes for the insulator. Each band contributes to the susceptibility with a term that is inversely proportional to the spin-wave velocity for that band. The low-temperature specific heat is proportional to T and to the sum of the inverses of the velocities of the four branches.

1. Introduction

The strongly anisotropic magnetic and transport properties of high-temperature superconductors arise primarily from the CuO planes. In particular, the high correlations among the electrons in the incomplete 3d shell of Cu are a key aspect for the understanding of these compounds. It has been conjectured [1] that the 1D and 2D variants of the Hubbard model have properties in common. There is some experimental evidence [2–6] that both the $3d_{x^2-y^2}$ and $3d_{z^2}$ orbitals may play a role in high-T_c cuprates. Motivated by this possibility, we consider an one-dimensional integrable model involving two equal nearest-neighbour tight-binding bands separated by a crystalline-field splitting, which could represent the two relevant orbitals. The electrons interact via a Hubbard-like repulsion, which provides the necessary intra- and interband correlations. Several multiband models have been previously proposed [7], including some integrable one-dimensional ones [8, 9]. Moreover, exact results in one dimension are often more accessible than two-dimensional ones and may provide a testing ground for approaches intended for more complex systems.

Our starting point is the generalization of Lieb and Wu's Bethe *ansatz* equations [10] for the one-dimensional spin-$\frac{1}{2}$ ($N = 2$) Hubbard model to N components with SU(N) symmetry [11–12]. For our two-band model there are four internal degrees of freedom, $N = 4$, composed of the direct product of the spin and the band indices. Several properties were derived for the ground state of the SU(N)-symmetric model. (i) The energy [13], the chemical potential [13], and the zero-field magnetic susceptibility, χ_S, [12, 13] were

0953-8984/95/010111+22$19.50

obtained as a function of band filling n, U and N. (ii) A small magnetic field gives rise to logarithmic singularities in the susceptibility as $H \to 0$ for all n, $U > 0$ and N [12, 13]. (iii) In the absence of external fields and as $N \to \infty$ the Bethe *ansatz* equation for the charges reduces to that of an interacting Bose gas. Contributions of order of $1/N$ vanish identically, so that the first corrections to leading order are of the order $1/N^2$ [12–15]. (iv) There is a qualitative change in the spectral density of the charge rapidities at a critical value of the coupling, U_c, which is associated with a metal–insulator transition of the Mott type [14]. Here U_c is a function of N, being zero for $N = 2$ [10] and it approaches 3.466 for $N \to \infty$. (v) The spectrum of elemental excitations, consisting of one branch of charge excitations and $(N-1)$ spin excitation branches arising from the internal degrees of freedom, shows the charge-colour separation characteristic of one-dimensional systems [13, 16]. (vi) The Fermi momentum of the charges, $p_F = \pi n$, is exclusively determined by the band filling and the momentum range of the spin waves is related to the Fermi surface of the charges [13]. (vii) The Fermi velocity, v_F, is finite for $U < U_c$ (metallic phase), diverges as $U \to U_c$ from below, and vanishes for $U > U_c$ (insulating phase) [14]. (viii) In the absence of external fields the spin-wave velocity, v_S, is the same for all the $(N-1)$ spin wave branches. v_S increases with the band filling n and decreases with U. For $U \to \infty$ the spin waves are soft, i.e. an infinitesimal field aligns all spins [13]. This is the consequence of an extended Pauli principle, since for $U = \infty$ no two electrons can occupy the same site. (ix) χ_S and v_S are inversely proportional; their product is independent of U and n [13]. (x) For $n = 1$ and large U the model maps onto the SU(N)-invariant Heisenberg chain [12, 17]. (xi) The low-T specific heat is proportional to T with proportionality constant $\gamma = (\pi/3)[1/v_F + (N-1)/v_S]$. (xii) In the continuum limit the charges interact with each other with an effective potential proportional to $[\sinh(ax)]^{-2}$, where x is the distance between the particles involved and a is an inverse length scale [14, 18]. (xiii) The Bethe eigenfunctions do not form a complete set of states [11, 14] and do not span the entire Fock space of the degenerate Hubbard model. Hence, an analytic form for the Hamiltonian of this model is not known. (xiv) The critical exponents determining the asymptotic behaviour of correlation functions at long distances and $T = 0$ were derived using conformal field theory in [19].

In this paper we consider a Hubbard-like model with two bands of equal hopping matrix element split by a crystal field, Δ. Our model is defined via the generalization of Lieb and Wu's Bethe *ansatz* solution [10] of the traditional Hubbard model to N internal degrees of freedom [11, 12]. Since the band splitting leaves the Bethe eigenfunctions unchanged, our system is then basically the generalization to $N = 4$. Unfortunately, as discussed above under point (xiii), an analytic expression of the Hamiltonian is not known. In section 2 we restate the SU(4) generalization [11, 12] of Lieb and Wu's Bethe *ansatz* equations of the Hubbard model [10], which define the model in terms of the Bethe eigenfunctions and their energies. We limit ourselves to the most important equations, which are the basis of our analysis. In section 3 we discuss the ground-state properties for one electron per site as a function of the population of the excited band. In particular, we focus on the phase diagram for the metal–insulator transition, which is characterized by the vanishing of the charge density of states at the Fermi level. The ground-state energy and the chemical potential are also obtained. The spectrum of elemental excitations is derived in section 4. There are four branches of elemental excitations: (i) charge excitations, (ii) interband or crystal-field transitions and (iii) two branches of spin waves. The Fermi velocity of the charges is finite in the metallic phase, diverges as the metal–insulator transition is approached from the metallic side and vanishes for the insulator. In section 5 we discuss the magnetic susceptibility and the low-temperature specific heat. Each band contributes to the susceptibility with a term

that is inversely proportional to the spin-wave velocity for that band. The specific heat is proportional to T and to the sum of the inverses of the velocities of the four branches of elemental excitations. Concluding remarks follow in section 6.

2. The Bethe *ansatz* equations

As pointed out in the introduction the model is defined through the SU(4) generalization of Lieb and Wu's Bethe *ansatz* equations. The Bethe eigenfunctions do not represent a complete set of states for the degenerate Hubbard model [11, 14]. The Hamiltonian form for our model is therefore not known and the model is simply defined as the collection of Bethe eigenstates and their energies. Below, after stating the SU(4) Bethe equations, we discuss which limits of the degenerate Hubbard model are recovered exactly.

Within the framework of Bethe's *ansatz* an integrable one-dimensional system of particles with four internal degrees of freedom (direct product of spin and number of bands) is parametrized in terms of one set of charge rapidities $\{k_j\}$, two sets of spin-rapidities describing the possible magnetization of each of the bands, $\{\xi_\alpha^{(l)}\}$, $l = 1, 3$, and one set of rapidities, $\{\Lambda_\alpha\}$, representing the crystalline-field splitting between the bands. Here j and α are running indices within these sets, $j = 1, ..., N_e$, N_e being the total number of electrons, and $\alpha = 1, ..., M^{(l)}$ for $l = 1, 2, 3$. Each internal degree of freedom gives rise to one set of rapidities. All rapidities within a given set have to be different for the wavefunctions to be linearly independent. This property leads to Fermi statistics for all the rapidities. The rapidities are not independent of each other but coupled by the discrete Bethe *ansatz* equations [11]

$$\exp\left(iN_a k_j\right) = \prod_{\alpha=1}^{M^{(1)}} \frac{\sin k_j - \xi_\alpha^{(1)} + iU/4}{\sin k_j - \xi_\alpha^{(1)} - iU/4} \qquad j = 1, ..., N_e \tag{2.1a}$$

$$\prod_{j=1}^{N_e} \frac{\xi_\alpha^{(1)} - \sin k_j - iU/4}{\xi_\alpha^{(1)} - \sin k_j + iU/4} \prod_{\beta=1}^{M^{(2)}} \frac{\xi_\alpha^{(1)} - \Lambda_\beta - iU/4}{\xi_\alpha^{(1)} - \Lambda_\beta + iU/4} = -\prod_{\beta=1}^{M^{(1)}} \frac{\xi_\alpha^{(1)} - \xi_\beta^{(1)} - iU/2}{\xi_\alpha^{(1)} - \xi_\beta^{(1)} + iU/2}$$
$$\alpha = 1, ..., M^{(1)} \tag{2.1b}$$

$$\prod_{\beta=1}^{M^{(1)}} \frac{\Lambda_\alpha - \xi_\beta^{(1)} - iU/4}{\Lambda_\alpha - \xi_\beta^{(1)} + iU/4} \prod_{\beta=1}^{M^{(3)}} \frac{\Lambda_\alpha - \xi_\beta^{(3)} - iU/4}{\Lambda_\alpha - \xi_\beta^{(3)} + iU/4} = -\prod_{\beta=1}^{M^{(2)}} \frac{\Lambda_\alpha - \Lambda_\beta - iU/2}{\Lambda_\alpha - \Lambda_\beta + iU/2}$$
$$\alpha = 1, ..., M^{(2)} \tag{2.1c}$$

$$\prod_{\beta=1}^{M^{(2)}} \frac{\xi_\alpha^{(3)} - \Lambda_\beta - iU/4}{\xi_\alpha^{(3)} - \Lambda_\beta + iU/4} = -\prod_{\beta=1}^{M^{(3)}} \frac{\xi_\alpha^{(3)} - \xi_\beta^{(3)} - iU/2}{\xi_\alpha^{(3)} - \xi_\beta^{(3)} + iU/2} \qquad \alpha = 1, ..., M^{(3)} \tag{2.1d}$$

where N_a is the number of sites in the chain. This solution corresponds to the Young tableau $(N_e - M^{(1)}, M^{(1)} - M^{(2)}, M^{(2)} - M^{(3)}, M^{(3)})$, where necessarily $N_a \geqslant N_e \geqslant M^{(1)} \geqslant M^{(2)} \geqslant M^{(3)} \geqslant 0$. The energy, the number of electrons populating the ground and excited bands ($n_g N_a$ and $n_e N_a$), and the magnetization are given by

$$E = -\sum_{j=1}^{N_e} 2\cos(k_j) \tag{2.2a}$$

$$n_g N_a = N_e - M^{(2)} \qquad n_e N_a = M^{(2)} \tag{2.2b}$$

$$S_z = (1/2)\Big(N_e + 2M^{(2)} - 2M^{(1)} - 2M^{(3)}\Big). \tag{2.2c}$$

The SU(4) generalization of the Lieb and Wu Bethe *ansatz* equations [11] contains the following limits. (i) For $M^{(2)} = M^{(3)} = 0$ the solution of the standard spin-$\frac{1}{2}$ Hubbard model is recovered; this corresponds to the excited-electron band being totally depopulated. (ii) In the limit $U \to 0$, $k_j N_a$ is an integer multiple of π and (2.1) reduce to the solution for free fermions with tight-binding dispersion. (iii) In the limit $U \to \infty$, again $k_j N_a$ is an integer multiple of π. Since the multiple occupation of a site is forbidden, the charges have a tight-binding dispersion and the internal degrees of freedom are all degenerate (no dispersion). (iv) In the continuum limit, i.e. $\sin(k) \approx k$, equations (2.1) reduce to those of a four-component Fermi gas interacting via a δ-function potential [20]. Hence, although the Hamiltonian form of the model is not known, it contains the relevant limiting cases and the interaction is in general of short-range character [14]. This makes equations (2.1) a physically meaningful model worth studying.

In the ground state all rapidities are real. We take logarithms of equations (2.1) and differentiate with respect to the variable k_j in (2.1*a*), $\xi_\alpha^{(1)}$ in (2.1*b*), Λ_α in (2.1*c*), and $\xi_\alpha^{(3)}$ in (2.1*d*). In the thermodynamic limit the rapidities are closely spaced and can be regarded as a continuous variable. Due to the tight-binding band, the k values are limited to the interval $[-\pi, \pi]$, while the other rapidities are not constrained. We introduce distribution density functions for the four sets of rapidities: $\rho(k)$ for the charges, $\sigma_2(\Lambda)$ for the crystalline-field rapidities and $\sigma_1(\xi)$ and $\sigma_3(\xi)$ for the spin rapidities. Similarly, we define the complementary 'hole' density functions for the states that are not occupied, $\rho_h(k)$, $\sigma_{2h}(\Lambda)$, $\sigma_{1h}(\xi)$ and $\sigma_{3h}(\xi)$. In the ground state the density distributions are symmetric functions of their arguments with $\rho(k)$ vanishing for $|k| > Q$, $\sigma_2(\Lambda) \equiv 0$ for $|\Lambda| > B$, and $\sigma_l(\xi) \equiv 0$ if $|\xi| > B_l$ for $l = 1, 3$. The density functions satisfy the following set of linear integral equations [11–13]:

$$\begin{aligned}\rho_h(k) + \rho(k) = \frac{1}{2\pi} &+ \cos k \int_{-Q}^{Q} \mathrm{d}k'\ G_1(\sin k - \sin k')\ \rho(k') \\ &+ \cos k \int_{-B}^{B} \mathrm{d}\Lambda\ G_1(\Lambda - \sin k)\ \sigma_2(\Lambda) \\ &- \cos k \int_{|\xi|>B_1} \mathrm{d}\xi\ G_0(\xi - \sin k)\ \sigma_{1h}(\xi)\end{aligned} \tag{2.3a}$$

$$\begin{aligned}\sigma_{1h}(\xi) + \sigma_1(\xi) = &\int_{|\xi'|>B_1} \mathrm{d}\xi'\ G_1(\xi' - \xi)\ \sigma_{1h}(\xi') + \int_{-Q}^{Q} \mathrm{d}k\ G_0(\xi - \sin k)\ \rho(k) \\ &+ \int_{-B}^{B} \mathrm{d}\Lambda\ G_0(\xi - \Lambda)\ \sigma_2(\Lambda)\end{aligned} \tag{2.3b}$$

$$\begin{aligned}\sigma_{2h}(\Lambda) + \sigma_2(\Lambda) = &\int_{-B}^{B} \mathrm{d}\Lambda' \Big[G_1(\Lambda - \Lambda') - G_3(\Lambda - \Lambda')\Big]\sigma_2(\Lambda') \\ &+ \int_{|\xi|>B_1} \mathrm{d}\xi\ G_0(\xi - \Lambda)\ \sigma_{1h}(\xi) + \int_{|\xi|>B_3} \mathrm{d}\xi\ G_0(\xi - \Lambda)\ \sigma_{3h}(\xi) \\ &+ \int_{-Q}^{Q} \mathrm{d}k\ G_1(\sin k - \Lambda)\ \rho(k)\end{aligned} \tag{2.3c}$$

$$\sigma_{3h}(\xi)+\sigma_3(\xi)=\int_{|\xi'|>B_3} d\xi'\ G_1(\xi'-\xi)\ \sigma_{3h}(\xi') + \int_{-B}^{B} d\Lambda\ G_0(\xi-\Lambda)\ \sigma_2(\Lambda) \tag{2.3d}$$

where

$$G_m(\Lambda)=\int_{-\infty}^{\infty}\frac{d\omega}{2\pi}\ e^{i\omega\Lambda}\ \frac{\exp(-m|\omega|U/4)}{2\cosh(\omega U/2)} = \mathrm{Re}\left\{\psi\left[\frac{m+3}{4}+i\frac{\Lambda}{U}\right]-\psi\left[\frac{m+1}{4}+i\frac{\Lambda}{U}\right]\right\}\frac{1}{\pi U} \tag{2.4}$$

with Re denoting *real part* and ψ being the digamma function.

The energy can be expressed as

$$E/N_a=-2\int_{-Q}^{Q} dk\ \cos(k)\ \rho(k) \tag{2.5a}$$

and the integration limits Q and B are determined by the number of electrons in each band, $n_g \geqslant n_e$,

$$n=n_g+n_e=\int_{-Q}^{Q} dk\ \rho(k) \qquad n_e=\int_{-B}^{B} d\Lambda\ \sigma_2(\Lambda). \tag{2.5b}$$

We define energy potentials, $\epsilon(k)$, $\varphi^{(2)}(\Lambda)$ and $\varphi^{(l)}(\xi)$, $l=1,3$, via

$$\begin{aligned}\epsilon(k)&=\lim_{T\to 0} T\ln\left[\rho_h(k)/\rho(k)\right]\\ \varphi^{(2)}(\Lambda)&=\lim_{T\to 0} T\ln\left[\sigma_{2h}(\Lambda)/\sigma_2(\Lambda)\right]\\ \varphi^{(l)}(\xi)&=\lim_{T\to 0} T\ln\left[\sigma_{lh}(\xi)/\sigma_l(\xi)\right]\end{aligned} \tag{2.6}$$

which are the energies entering the Fermi functions populating the bands. The potentials satisfy the following integral equations:

$$\epsilon(k)=-2\cos(k)-\mu+\int_{-Q}^{Q} dk'\ \cos k'\ G_1(\sin k-\sin k')\ \epsilon(k') + \int_{-B}^{B} d\Lambda\ G_1(\Lambda-\sin k)\ \varphi^{(2)}(\Lambda) - \int_{|\xi|>B_1} d\xi\ G_0(\xi-\sin k)\ \varphi^{(1)}(\xi) \tag{2.7a}$$

$$\varphi^{(1)}(\xi)=H/2+\int_{|\xi'|>B_1} d\xi'\ G_1(\xi'-\xi)\ \varphi^{(1)}(\xi')+\int_{-Q}^{Q} dk\ \cos k\ G_0(\xi-\sin k)\ \epsilon(k) + \int_{-B}^{B} d\Lambda\ G_0(\xi-\Lambda)\ \varphi^{(2)}(\Lambda) \tag{2.7b}$$

$$\varphi^{(2)}(\Lambda) = \Delta + H + \int_{-B}^{B} d\Lambda' \Big[G_1(\Lambda - \Lambda') - G_3(\Lambda - \Lambda') \Big] \varphi^{(2)}(\Lambda') + \int_{-Q}^{Q} dk \cos k \; G_1(\sin k - \Lambda) \; \epsilon(k) - \int_{|\xi|>B_1} d\xi \; G_0(\xi - \Lambda) \; \varphi^{(1)}(\xi) - \int_{|\xi|>B_3} d\xi \; G_0(\xi - \Lambda) \; \varphi^{(3)}(\xi) \tag{2.7c}$$

$$\varphi^{(3)}(\xi) = H/2 + \int_{|\xi'|>B_3} d\xi' \; G_1(\xi' - \xi) \; \varphi^{(3)}(\xi') + \int_{-B}^{B} d\Lambda \; G_0(\xi - \Lambda) \; \varphi^{(2)}(\Lambda) \tag{2.7d}$$

where μ is the chemical potential and Δ is the band splitting. The potentials are symmetric and increasing functions of $|k|$, $|\Lambda|$ and $|\xi|$, respectively. The zeros of the potentials, $\epsilon(\pm Q) = 0$, $\varphi^{(2)}(\pm B) = 0$ and $\varphi^{(l)}(\pm B_l) = 0$, define the relation of Q, B and B_l with μ, Δ and H. The above equations are valid for $n \leqslant 1$, all U, Δ and H.

In the absence of a magnetic field the spin rapidities $\xi^{(l)}$ fill the entire real axis, $B_1 = B_3 = \infty$, and can be eliminated from the problem. In this limit the potentials $\varphi^{(l)}(\xi)$, $l = 1, 3$, are negative for all ξ and the spin-rapidity bands are completely filled.

3. Ground-state properties

We now restrict ourselves to a band filling of exactly one electron per site, $n = N_e/N_a = 1$ and zero magnetic field. Only for $n = 1$ may the system undergo a metal–insulator transition. The integral equations for the densities and the potentials reduce then to a system of two coupled equations, which can be solved numerically by discretizing the integrals using about 100 points.

Depending on the interaction strength U and the band splitting Δ, not all Q values between zero and π are necessarily meaningful [13, 14]. This is best seen from the $U = 0$ limit presented in the appendix. For $U = 0$ the chain is metallic with $\pi/4 \leqslant Q \leqslant \pi/2$ depending on the relative populations of the electron bands. In the k range where both bands are occupied $\rho(k) = 2/\pi$, while $\rho(k) = 1/\pi$ if only the lower-lying electron band is populated. For $U \to \infty$, on the other hand, we have an insulator with $\rho(k) = 1/(2\pi)$ and $Q = \pi$. In this case each k value can only be occupied once. $\rho(k)$ and $\rho_h(k)$ are symmetric and non-negative (since they represent a density of states) functions of their argument k. If we increase U, starting from $U = 0$ and assuming $B \neq 0$, the repulsion is unfavourable to a multiple occupation of sites, leading to a gradual increase of Q. The system remains metallic until $Q = \pi$ is reached. This occurs at a critical value U_c of the coupling, which corresponds to the Mott transition [14]. Hence, for $U < U_c$ the system is metallic, while for $U > U_c$ it is insulating. A similar behaviour is obtained if B is decreased with U kept constant. Figure 1 shows $\rho(k)$ as a function of k for $U = 2.5$, $N_e = N_a$ and several values of n_e (or B). In general $\rho(k)$ has a maximum at $k = 0$, since for small k both electron bands have the highest probability of occupation. Curves (a) and (b) correspond to the insulating phase with $Q = \pi$, curves (d) and (e) represent two metallic situations, while (c) is the point of the metal–insulator transition. At the Mott transition $\rho(Q = \pi)$ vanishes indicating that the charges cease to have a Fermi surface. $\rho(Q = \pi)$ is non-zero elsewhere. This zero

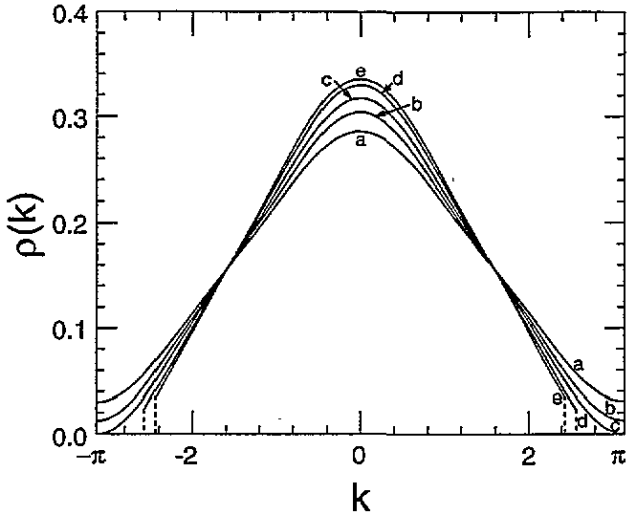

Figure 1. Density distribution of charge rapidities $\rho(k)$ for one electron per site ($n = 1$), $U = 2.5$ and five values of n_e: (a) 0.0, (b) 0.1088, (c) 0.2017, (d) 0.3326 and (e) 0.50. For cases (a), (b) and (c) $Q = \pi$, while in cases (d) and (e) $Q = 2.572$ and 2.440, respectively. Cases (a) and (b) represent insulating situations, while for (d) and (e) the system is a metal. Case (c) corresponds to the Mott metal–insulator transition. Note that $\rho(Q)$ is finite in all cases except (c). The vanishing of the density of states at the Fermi point characterizes the Mott transition. $\rho(k)$ is finite everywhere for $|k| \leqslant Q$ if $n < 1$. Note that $\rho(k)$ has a maximum for $k = 0$; this indicates that a multiple occupancy of a small-$|k|$ state is more likely than for larger $|k|$ (single occupancy corresponds to $\rho = 1/(2\pi)$). Also, the larger n_e the larger the small-$|k|$ occupation probability.

of $\rho(Q)$ has consequences on the Fermi velocity of the elemental charge excitations [14] (see section 4). $\rho(Q)$ is of course finite for all U and Δ if $n < 1$.

For $N_e = N_a$ the integration limits B and Q are not independent. Figure 2(A) shows their interrelation for several values of U. For $U > 2.981$ we have $Q = \pi$ for all B and the system is always an insulator. For $U = 0$ only B values smaller than $2^{-1/2}$ are allowed. For $U < 2.981$ the slope, dQ/dB, diverges as the Mott transition is approached from the metallic side, $Q \to \pi$. The population of the excited-electron band as a function of B for various U is displayed in figure 2(B). The limit $B = 0$ corresponds to an empty excited band ($n_e = 0$), that is, to the standard spin-$\frac{1}{2}$ Hubbard model, which is an insulator for all $U > 0$. The occupation of the lower-lying electron band is $n_g = 1 - n_e$. The density of charge states for $k = \pm Q$ is displayed in figure 3(A) as a function of n_e for several U. For $U = \infty$ we have $\rho(Q = \pi) = 1/(2\pi)$. The quantity $\rho(\pi)$ decreases monotonically with decreasing U and/or increasing n_e. For $U > 2.981$ the quantity $\rho(\pi)$ is always positive and the chain is insulating. The behaviour changes when U is decreased further, where $\rho(\pi) = 0$ for a specific value of n_e^c (which depends on U). As discussed above this corresponds to the Mott metal–insulator transition. For $U = 2.5$ the transition occurs at $n_e^c = 0.2017$, for $U = 2$ at $n_e^c = 0.0884$ and for $U = 1$ at $n_e^c = 0.00264$. If n_e is smaller than this specific value n_e^c the system is insulating, while if $n_e > n_e^c$ it is metallic. In figure 3(B) we show the metal–insulator boundary as a function of the population of the excited-electron band. For $U > U_c$ the chain is insulating, otherwise it is metallic. As $n_e \to 0.5$ the bands become degenerate, $n_g = n_e$, and $U_c = 2.981$. For $n_e = 0$ one band is completely empty and the other one half filled; this corresponds to the standard Hubbard model with $U_c = 0$. For

small n_e we obtain that along the phase boundary $n_e = B/\pi \approx U_c^{1/2}\exp(-2\pi/U_c)$, i.e., the dependence is non-analytic as $U \to 0$.

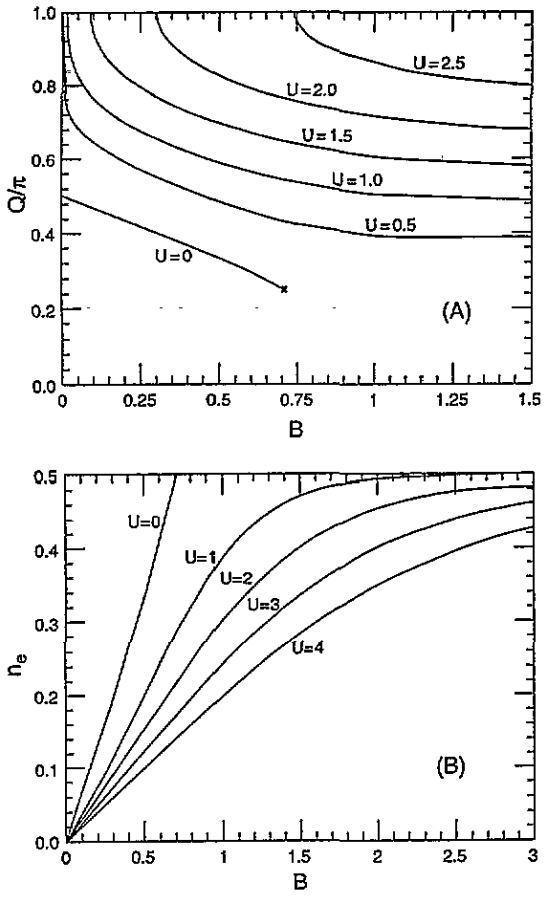

Figure 2. (A) Relation between the integration limits Q and B for $n = 1$ (one electron per site) and several values of U. For $U = 0$ the range of B is restricted to values smaller than $2^{-1/2}$, while $\pi/4 \leqslant Q \leqslant \pi/2$. $Q = \pi$ for all B for $U > 2.981$. If $Q = \pi$ the system is an insulator, while for $Q < \pi$ the chain is metallic. The metal–insulator transition occurs at the points where $Q \to \pi$ (with infinite slope). (B) Occupation of the excited band, n_e, as a function of B for $n = 1$ and several U values. If $B = 0$ the excited band is empty, and with increasing B the value of $n_e = 0.5$ is asymptotically reached. Note the qualitatively different behaviour for $U = 0$.

The ground-state energy, the chemical potential and the band splitting, Δ, are displayed in figure 4 as a function of n_e for various U values and $N_e = N_a$. Both the energy and μ increase with increasing U and decrease with increasing n_e. Δ, on the other hand, decreases monotonically as both U and n_e increase. For $U = 0$ and $n_e = 0$ the chemical potential vanishes and the band splitting is equal two (one electron band is half filled, the other one is empty). For $U \to \infty$ the ground-state energy is zero, and μ is equal to two. In this limit two electrons are not allowed to occupy the same site and an infinitesimal Δ completely depopulates the excited-electron band. For $n_e = n_g = 0.5$, on the other hand, both bands are degenerate and necessarily $\Delta = 0$. Along the phase boundary we have, for small U,

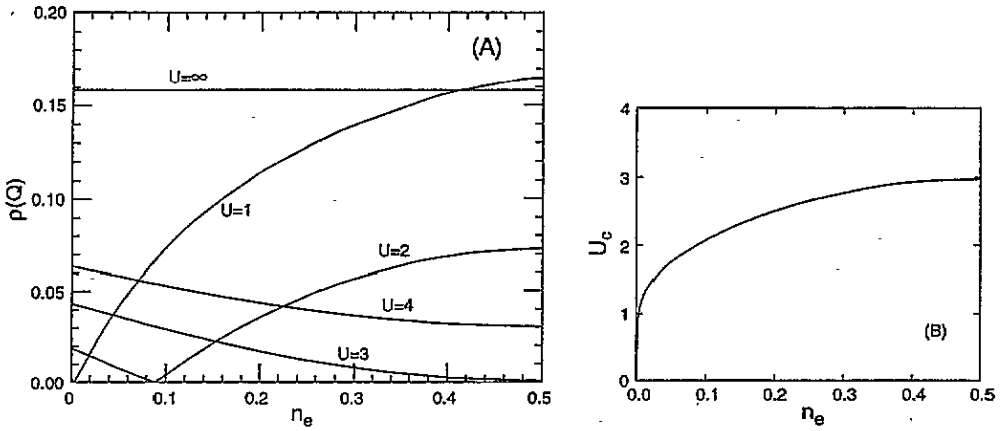

Figure 3. (A) Density of charges at the 'Fermi surface', $\rho(Q)$, for $n = 1$ and several U values as a function of n_e. For $U \to \infty$ the density equals $1/(2\pi)$ everywhere, while for $U = 0$ we have $\rho(Q) = 1/\pi$ if $n_e \neq 0.5$ and $\rho(Q) = 2/\pi$ if $n_e = 0.5$. $\rho(Q) > 0$ for all n_e if $U > 2.981$; in this case the system is always an insulator. For $U < 2.981$, $\rho(Q)$ has a zero at a given value of n_e, denoted by n_e^c. This point corresponds to the metal–insulator transition. For $n_e > n_e^c$ the chain is metallic, while for $n_e < n_e^c$ it is insulating. (B) Phase diagram for the Mott transition: $U_c = 0$ if $n_e = 0$ (standard spin-$\frac{1}{2}$ Hubbard model), and $U_c = 2.981$ for $n_e = 0.5$ (degenerate bands, SU(4)-symmetric Hubbard model). As $U \to 0$ the dependence is non-analytic, $n_e \approx U_c^{1/2}\exp(-2\pi/U_c)$.

that $\Delta = 2 - U_c/2$. The metal–insulator transition is only seen as a change in slope of the chemical potential, e.g. for $U = 2$ at $n_e = 0.088\,39$.

4. Elemental excitations

In this section we study the spectrum of elemental excitations obtained by adding or removing one rapidity from one of the four sets of rapidities [13, 21, 22]. The spectrum of elemental excitations consists of (i) one branch of charge excitations, (ii) one branch of crystalline-field excitations and (iii) two branches of spin waves. Since the equations determining the densities of rapidities, (2.3), and the energy potentials for the rapidities, (2.6), are linear integral equations, the superposition principle holds for any finite number of excitations, i.e., the excitations have a soliton-like behaviour. The excitation energies and their momenta are additive. In view of the spin and charge separation in one dimension, actual excitations, e.g. electron–hole excitations or interband transitions, are built up as combinations of elemental excitations and give rise to a continuum of excitations for a given momentum [13, 21, 22]. In addition, the Hubbard model has more complex excitations given by strings of complex rapidities [23], which do not contribute to the very-low-temperature behaviour and are not discussed here.

(i) Charge excitations are obtained by removing a charge rapidity k_0 from the system. For one electron per site there are only hole excitations, since the k band is filled and no further charge can be added. Removing the charge rapidity gives rise to a rearrangement of the remaining rapidities and hence to a change in the energy $\Delta E_{ch}(k_0)$, which is given by the corresponding energy potential,

$$\Delta E_{ch}(k_0) = |\epsilon(k_0)| = -\epsilon(k_0). \tag{4.1a}$$

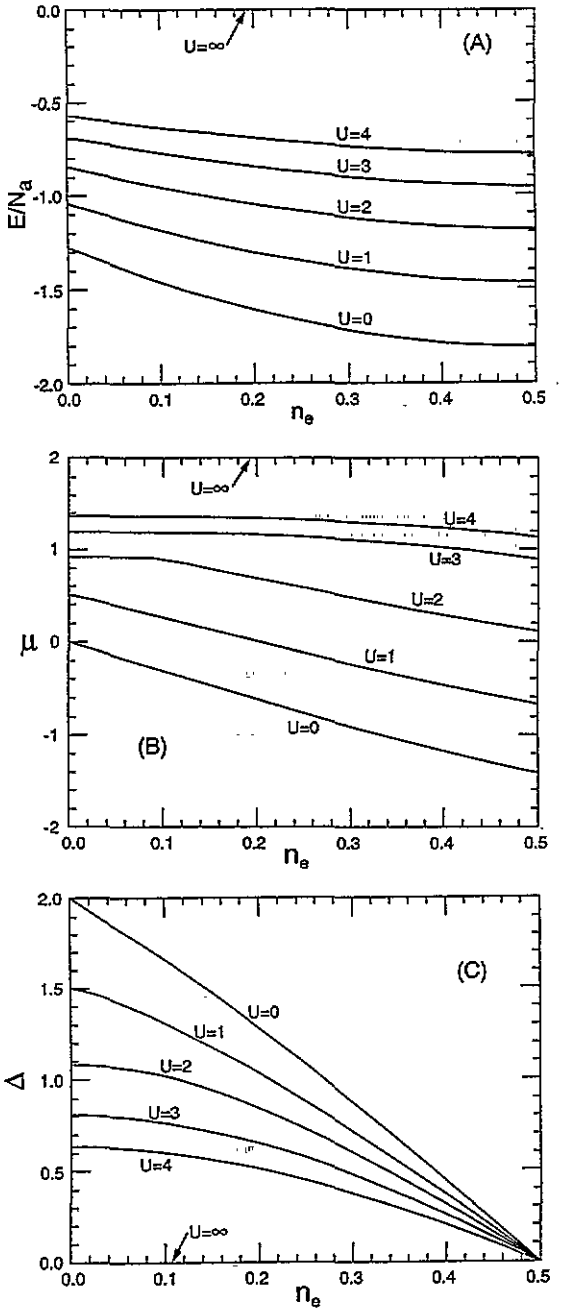

Figure 4. (A) Ground-state energy, E/N_a, (B) chemical potential, μ, and (C) crystalline-field band splitting, Δ, as a function of n_e for $n = 1$ and several values of U. For $U \to \infty$ all sites are singly occupied and we have $E/N_a = 0$, $\mu = 2$ and $\Delta = 0$. Note that the metal–insulator transition is seen as a change of slope of μ at n_e^c, e.g. at $n_e = 0.088\,39$ for $U = 2$ and at $n_e = 0.002\,645$ for $U = 1$.

Although the charge rapidities are frequently called momenta, they do not represent the physical momenta of the particles and holes. The physical momentum of the excitation is

related to the density function via

$$p_{ch}(k_0) = 2\pi \int_0^{k_0} dk\ \rho(k). \tag{4.1b}$$

With this definition a charge removed from the centre of the Brillouin zone ($k_0 = 0$) has zero momentum and a rapidity removed from the zone boundary, $k_0 = \pm Q$, has momentum $p_{ch} = \pm\pi$ (one electron per site).

It is instructive to discuss the $U \to 0$ and $U \to \infty$ limits. For $U \to 0$ we obtain (see the appendix) for $N_e = N_a$

$$\Delta E_{ch}(k_0) = \begin{cases} 8\cos(k_0) + 4\mu - 2\Delta & \text{if } |\sin(k_0)| \leqslant B \\ 4\cos(k_0) + 2\mu & \text{if } B < |\sin(k_0)| \leqslant \sin(Q) \end{cases} \tag{4.2a}$$

$$p_{ch}(k_0) = \begin{cases} 4k_0 & \text{if } |\sin(k_0)| \leqslant B \\ 2\sin^{-1}(B) + 2k_0 & \text{if } B < |\sin(k_0)| \leqslant \sin(Q). \end{cases} \tag{4.2b}$$

In the limit $U \to \infty$, on the other hand,

$$\Delta E_{ch}(k_0) = 2\cos(k_0) + \mu \qquad p_{ch}(k_0) = k_0 \tag{4.3}$$

which corresponds to free spinless fermions on a tight-binding lattice.

The dispersion of the charge-hole excitations is seen in figure 5(A) for $U = 2.5$ and the same values of n_e as in figure 1. The excitation energy is maximum at the centre of the Brillouin zone and vanishes at the zone boundary. All curves are similar, although there are some qualitative differences. In the insulating phase (cases (a) and (b)) $\Delta E_{ch}(p = 0) = 4$, while this value is less than four in the metallic phase (cases (d) and (e)). Note also that the slope of $\Delta E_{ch}(p)$ (Fermi velocity) is finite at $p = \pm\pi$ for the metal, while it vanishes for the insulator. Case (c) corresponds to the point of the Mott transition. The Fermi velocity of the charge can explicitly be obtained via

$$v_F = \frac{d\epsilon(k)}{dk}\Big|_Q \Big/ 2\pi\rho(Q)\ . \tag{4.4}$$

Here the derivative of ϵ is obtained as

$$\frac{d\epsilon(k)}{dk}\Big|_Q = 2\sin(Q) + \cos(Q)\int_{-Q}^{Q} dk'\ \cos(k')\ \epsilon(k')\ \tilde{G}_1(\sin(Q) - \sin k') + \cos(Q)\int_{-B}^{B} d\Lambda\ \varphi_2(\Lambda)\ \tilde{G}_1(\sin(Q) - \Lambda) \tag{4.5a}$$

where

$$\tilde{G}_m(\Lambda) = -\frac{1}{\pi U^2}\mathrm{Im}\left\{\psi'[(m+3)/4 + i\Lambda/U] - \psi'[(m+1)/4 + i\Lambda/U]\right\} \tag{4.5b}$$

with ψ' being the trigamma function. The derivative vanishes in the insulating phase where $Q = \pi$ and so does the Fermi velocity. In the metallic phase, where $Q < \pi$, the derivative, and hence v_F, are finite. $\rho(Q)$ tends to zero as the metal–insulator transition is approached from the metallic side giving rise to a divergent Fermi velocity. v_F as a function of n_e for

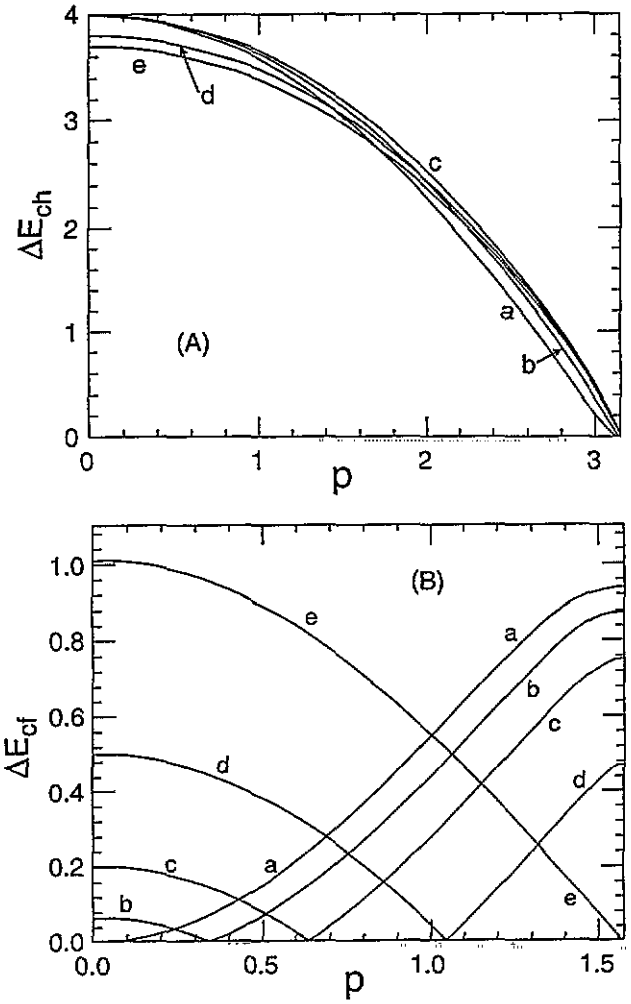

Figure 5. Spectrum of elemental excitations for one electron per site ($n = 1$), $U = 2.5$ and five values of n_e: (a) 0.0, (b) 0.1088, (c) 0.2017, (d) 0.3326 and (e) 0.50. The cases (a) and (b) represent insulating situations, while for (d) and (e) the system is a metal. Case (c) corresponds to the Mott metal–insulator transition. (A) Charge-'hole' excitations obtained by removing a charge rapidity from the system. Note that $\Delta E_{ch}(p = 0) = 4$ for the insulator, while $\Delta E_{ch}(p = 0) < 4$ in the metallic situation. The Fermi velocity (slope at $p = \pi$) is finite for the metal and zero for the insulator. The Fermi momentum is πn. (B) Crystalline-field excitation obtained by adding or removing a Λ rapidity. The excitation energy vanishes at the Fermi surface for the crystalline-field excitations of Fermi momentum $p_{cfF} = \pi n_e$. Excitations with momentum larger than p_{cfF} are 'holes', while those with momentum smaller than πn_e correspond to 'particles'. Except for the empty band ($n_e = 0$) the crystal-field velocity is non-zero. (C) Spin-wave excitations within the lower-lying electron band. The maximum momentum is $\pi(n+n_e)$. In zero magnetic field there are only 'hole' excitations, since the spin-rapidity band is full. The slope for small p defines the spin-wave velocity $v_{sw}^{(1)}$. (D) Spinwave excitations within the excited-electron band. The maximum momentum is πn_e and there are only 'hole' excitations, since the spin-rapidity band is full. For $n_e = 0$ the spectrum shrinks to one point (empty band). The slope for small p defines the spin-wave velocity $v_{sw}^{(3)}$.

several values of U is shown in figure 6(A). The system is always metallic if $U = 0$, is insulating for small n_e if $0 < U < 2.981$ and is always insulating if $U > 2.981$.

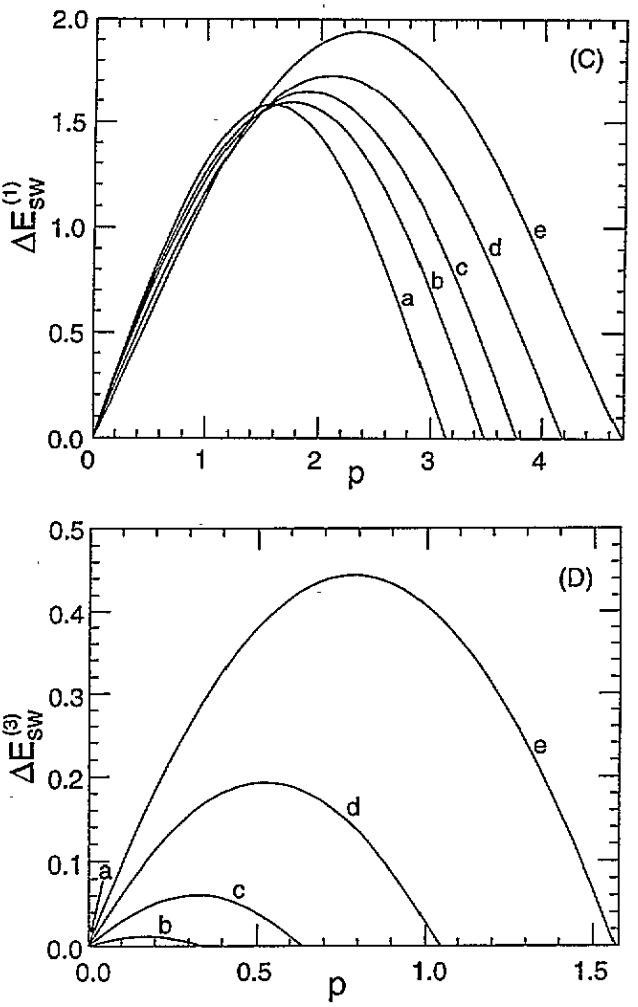

Figure 5. (Continued)

(ii) The crystalline-field excitations are obtained by adding (particle excitation, $|\Lambda_0| > B$) or removing (hole excitation, $|\Lambda_0| < B$) the rapidity Λ_0. This slightly rearranges the k rapidities and gives rise to a change in energy

$$\Delta E_{cf}(\Lambda_0) = |\varphi^{(2)}(\Lambda_0)| \,. \tag{4.6a}$$

The Fermi surface for the crystalline-field excitations is defined by $\varphi_2(\pm B) = 0$. The momentum of the excitation is from its definition (assuming one electron per site)

$$\begin{aligned} p_{cf}(\Lambda_0) &= 2\pi \int_0^{\Lambda_0} d\Lambda \, [\sigma_2(\Lambda) + \sigma_{2h}(\Lambda)] \\ &= 2\int_{-B}^{B} d\Lambda \, \sigma_2(\Lambda) \, \mathrm{Im} \ln \left\{ \frac{\Gamma[1 + i(\Lambda_0 - \Lambda)/U]^2}{\Gamma[0.5 + i(\Lambda_0 - \Lambda)/U] \, \Gamma[1.5 + i(\Lambda_0 - \Lambda)/U]} \right\} \\ &\quad + 2\int_{-Q}^{Q} dk \, \rho(k) \, \mathrm{Im} \ln \left\{ \frac{\Gamma[1 + i(\Lambda_0 - \sin(k))/U]}{\Gamma[0.5 + i(\Lambda_0 - \sin(k))/U]} \right\} . \end{aligned} \tag{4.6b}$$

Again, the momentum is zero for a hole at the centre of the Brillouin zone, is $p_{cfF} = \pi n_e$ at the Fermi level and is $p_{cf} = \pi/2$ for $\Lambda_0 \to \infty$. The limit $U \to 0$ is easily obtained using the results from the appendix

$$\Delta E_{cf}(\Lambda_0) = \begin{cases} -2\Delta + 2\mu + 4\sqrt{1-\Lambda_0^2} & \text{if } |\Lambda_0| < B \\ \Delta - \mu - 2\sqrt{1-\Lambda_0^2} & \text{if } B < |\Lambda_0| < \sin(Q) \\ \Delta & \text{if } \sin(Q) < |\Lambda_0| \end{cases} \tag{4.7a}$$

$$p_{cf}(\Lambda_0) = \begin{cases} 2\sin^{-1}(\Lambda_0) & \text{if } |\Lambda_0| < B \\ \sin^{-1}(B) + \sin^{-1}(\Lambda_0) & \text{if } B < |\Lambda_0| < \sin(Q) \\ \pi/2 & \text{if } \sin(Q) < |\Lambda_0| \,. \end{cases} \tag{4.7b}$$

In the limit $U \to \infty$ the crystal field excitations are soft, i.e. the excitation energy is identically zero, since an arbitrarily small Δ already empties the excited electron band.

The spectrum of the crystalline-field excitations is seen in figure 5(B) for $U = 2.5$ and the same values of n_e as before. The excitation energy vanishes at the Fermi level with Fermi momentum πn_e. Case (a) corresponds to the empty rapidity band (standard spin-$\frac{1}{2}$ Hubbard model), case (c) refers to the metal–insulator transition and in case (e) the two electron bands are degenerate. The slope of the excitation energy at the Fermi level is finite everywhere except for $n_e = 0$. This crystalline-field velocity is shown in figure 6(B) as a function of n_e for several U. The different behaviour for $U = 0$ at small n_e is the consequence of the Mott transition, which for small but finite U takes place for small n_e. The velocity of the crystalline-field excitations is explicitly obtained via

$$v_{cf} = \frac{d\varphi^{(2)}(\Lambda)}{d\Lambda}\Big|_B \Big/ 2\pi\sigma_2(B) \tag{4.8a}$$

where the derivative of $\varphi^{(2)}$ is computed as

$$\frac{d\varphi^{(2)}(\Lambda)}{d\Lambda}\Big|_B = \int_{-Q}^{Q} dk\, \cos(k)\, \epsilon(k)\, \tilde{G}_1(B - \sin k) + \int_{-B}^{B} d\Lambda\, \varphi^{(2)}(\Lambda)\, \Big[\tilde{G}_1(B-\Lambda) - \tilde{G}_3(B-\Lambda)\Big]. \tag{4.8b}$$

(iii) The spin-wave excitations are obtained by removing one spin rapidity from one of the spin-rapidity sets. In the absence of a magnetic field the spin-rapidity bands are completely filled, so that there are only 'hole' excitations (the spin-rapidity potentials are negative everywhere). Removing the spin rapidity $\xi_0^{(l)}$ slightly rearranges the charge rapidities and gives rise to a change in energy,

$$\Delta E_{sw}^{(l)}(\xi_0) = |\varphi^{(l)}(\xi_0)| \tag{4.9a}$$

where $l = 1, 3$ refers to the two classes of spin-wave excitations. The energy potentials are obtained via (2.7) with $B_1 = B_3 = \infty$. The corresponding momenta are ($l = 1, 3$)

$$p_{sw}^{(l)}(\xi_0) = 2\pi \int_{-\infty}^{\xi_0} d\xi\, \sigma_l(\xi) = 2\int_{-B}^{B} d\Lambda\, \sigma_2(\Lambda)\, \tan^{-1}[\exp(2\pi(\xi_0 - \Lambda)/U)] + 2\,\delta_{l,1} \int_{-Q}^{Q} dk\, \rho(k)\, \tan^{-1}[\exp(2\pi(\xi_0 - \sin(k))/U)]. \tag{4.9b}$$

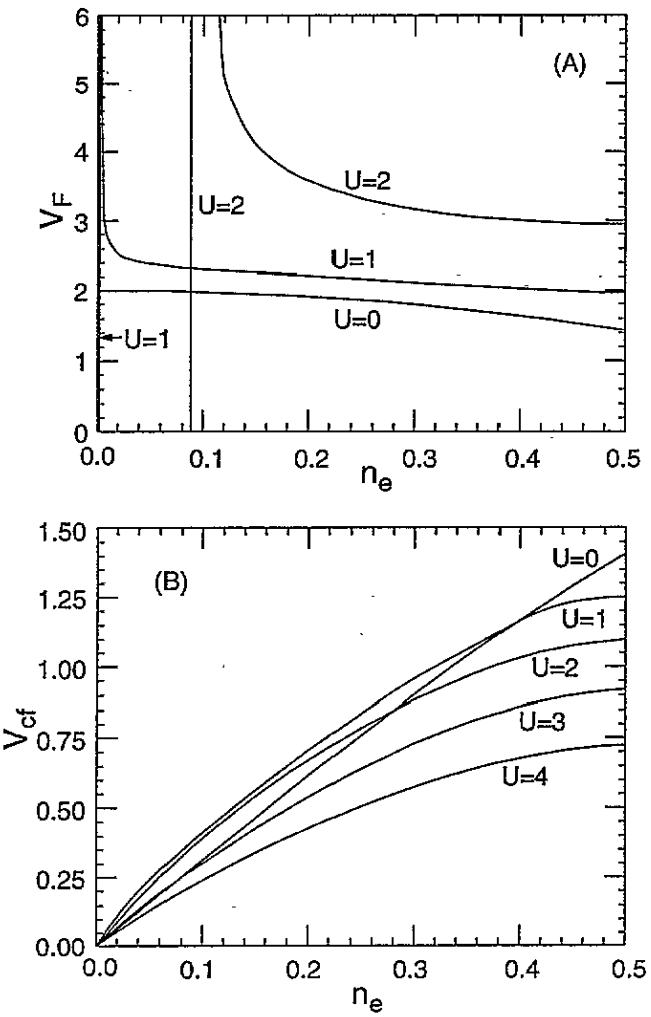

Figure 6. Group velocities of the elemental excitations as a function of n_e for one electron per site ($n = 1$) and several values of U. (A) The Fermi velocity of the charges, v_F, is zero in the insulating phase and finite if the system is a metal. v_F diverges when the Mott transition is approached from the metallic phase ($n_c^c = 0.002\,645$ for $U = 1$, $n_c^c = 0.088\,39$ for $U = 2$). (B) The group velocity of crystalline field excitations, v_{cf} vanishes when $n_e \to 0$ (empty excited-electron band). The velocity decreases with increasing U and vanishes for $U \to \infty$ (an arbitrarily small Δ depopulates the excited-electron band). The different behaviour for $U = 0$ at small n_e is a consequence of the metal–insulator transition. (C) Spin-wave velocity for excitations within the lower-lying electron band. The velocity increases with the number of electrons in the band ($n_g = 1 - n_e$). $v_{sw}^{(1)}$ is always finite since the electron band is always populated. $v_{sw}^{(1)}$ decreases with increasing U and vanishes as $U \to \infty$. (D) Spin-wave velocity for excitations within the excited-electron band. The velocity increases with the number of electrons in the band, n_e, and vanishes when $n_e = 0$. $v_{sw}^{(3)}$ decreases with increasing U and vanishes as $U \to \infty$.

$\Delta E_{sw}^{(l)}(\xi_0)$ are symmetric functions of ξ_0, which vanish as $\xi_0 \to \pm\infty$ and have their maximum at $\xi_0 = 0$. The ranges of the momenta of the spin waves depend on the band fillings and are given by the intervals $[0, \pi(2n_e + n_g)]$ for $l = 1$ and $[0, \pi n_e]$ for $l = 3$. In particular, since the $l = 3$ band refers to the spin waves in the excited-electron band, the

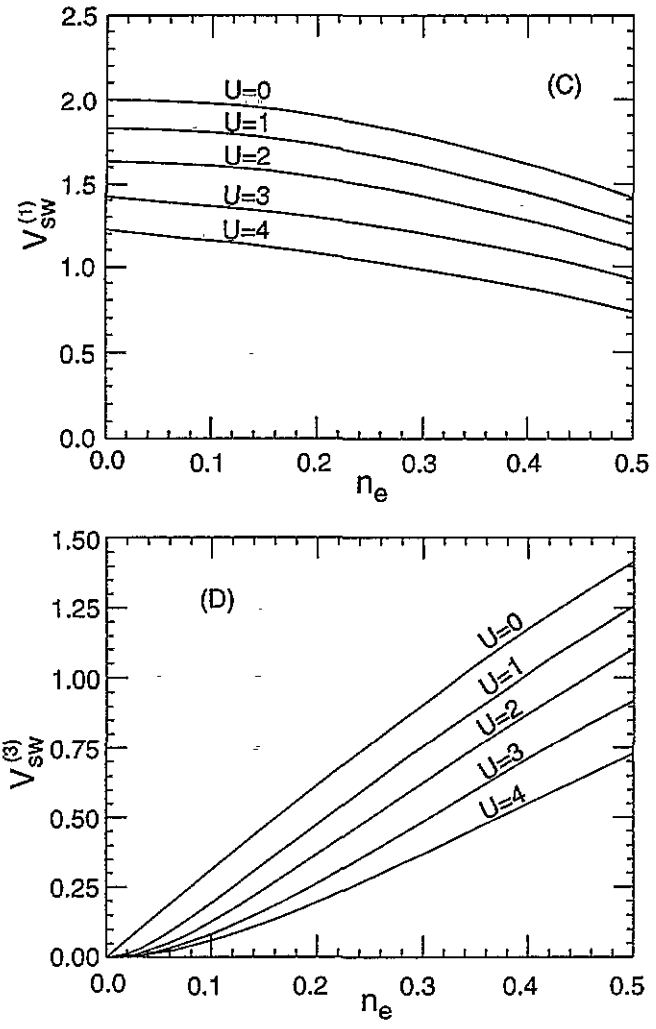

Figure 6. (Continued)

excitation energy and the momentum only depend on $\varphi^{(2)}$ and σ_2. The spin-wave dispersions are shown in figures 5(C) and 5(D) for $U = 2.5$, $n = 1$ and the same values of n_e as before. In case (a) the excited band is empty, so that there is no dispersion for $l = 3$. The maximum height of the dispersion decreases monotonically with n_e.

The slope at $p = 0$ is the spin-wave velocity, which can be obtained by expanding the energy and the momentum for $\xi_0 \to -\infty$. Both quantities vanish exponentially as $\xi_0 \to -\infty$ and after some algebra we obtain

$$v_{sw}^{(1)} = -\frac{1}{U}\frac{\int_{-Q}^{Q} dk\, \cos(k)\, \epsilon(k)\, \exp[-2\pi \sin k/U] + \int_{-B}^{B} d\Lambda\, \varphi^{(2)}(\Lambda)\, \exp[-2\pi \Lambda/U]}{\int_{-Q}^{Q} dk\, \rho(k)\, \exp[-2\pi \sin k/U] + \int_{-B}^{B} d\Lambda\, \sigma_2(\Lambda)\, \exp[-2\pi \Lambda/U]}$$

$$v_{sw}^{(3)} = -\frac{1}{U}\frac{\int_{-B}^{B} d\Lambda\, \varphi^{(2)}(\Lambda)\, \exp[-2\pi \Lambda/U]}{\int_{-B}^{B} d\Lambda\, \sigma_2(\Lambda)\, \exp[-2\pi \Lambda/U]} \tag{4.10}$$

The spin-wave velocities are displayed for $n = 1$ and several U values as a function of n_e in

figures 6(C) and 6(D), repectively. The spin-wave velocity increases with the population of the corresponding electron band. Hence, $v_{sw}^{(3)}$ monotonically increases with n_e and vanishes as n_e tends to zero (the excited-electron band is empty). On the other hand, $v_{sw}^{(1)}$ decreases with increasing n_e ($n_g = 1 - n_e$ decreases) and remains finite since the lower-lying electron band is always populated. The velocities also decrease as a function of U and vanish identically for $U \to \infty$ since the spin waves are soft (the excitation energies are identically zero). In this limit an infinitesimal magnetic field completely polarizes the electrons.

In the limit $U \to 0$ the excitation energies are (see the appendix)

$$\Delta E_{sw}^{(l)}(\xi_0) = \begin{cases} -2\Delta + 3\mu + 6\sqrt{1-\xi_0^2} & \text{if } |\xi_0| < B \\ +\mu + 2\sqrt{1-\xi_0^2} & \text{if } B < |\xi_0| < \sin(Q) \\ 0 & \text{elsewhere} \end{cases} \tag{4.11a}$$

$$\Delta E_{sw}^{(3)}(\xi_0) = \begin{cases} -\Delta + \mu + 2\sqrt{1-\xi_0^2} & \text{if } |\xi_0| < B \\ 0 & \text{elsewhere} \end{cases} \tag{4.11b}$$

and the momenta are obtained using the expressions for the densities given in the appendix

$$p_{sw}^{(l)}(\xi_0) = \pi \int_{-B}^{\xi_0} d\Lambda\ \sigma_2(\Lambda) + \delta_{l,1}\ \pi \int_{-Q}^{\sin^{-1}(\xi_0)} dk\ \rho(k). \tag{4.11c}$$

The four velocities are then $v_{sw}^{(1)} = v_F = 2\sin(Q)$ and $v_{sw}^{(3)} = v_{cf} = 2B$.

Finally we briefly address the limit $B \to \infty$, where the crystalline-field splitting is zero and the two bands are degenerate (SU(4) invariance). All rapidity bands are full in this limit and there are only 'hole' excitations. The potentials and the densities for the internal degrees of freedom are obtained by Fourier transformation (for Λ or ξ)

$$\varphi^{(l)}(\Lambda) = \int_{-Q}^{Q} dk\ \cos(k)\ \epsilon(k) \frac{1}{2U} \frac{\sin(\pi l/4)}{\cosh[\pi(\Lambda - \sin(k))/U] - \cos(\pi l/4)} \tag{4.12a}$$

$$\sigma^{(l)}(\Lambda) = \int_{-Q}^{Q} dk\ \rho(k) \frac{1}{2U} \frac{\sin(\pi l/4)}{\cosh[\pi(\Lambda - \sin(k))/U] - \cos(\pi l/4)} \tag{4.12b}$$

where $l = 1, 2, 3$. This reproduces results presented in [13].

5. Susceptibility and low-temperature specific heat

The low temperature specific heat is determined by the low-energy excitations. As a consequence of the Fermi statistics obeyed by all rapidities the low-T specific heat is proportional to the temperature. Only excitation branches of rapidities with a Fermi surface can contribute, that is, we have in general four contributions in the metallic case, but only three in the insulating situation where the charge degrees of freedom are frozen out. The temperature smears the Fermi surfaces of the rapidities and giving rise to a term with T^2 dependence in the energy potentials of the rapidities and the free energy, unless the

spectrum has a gap. The γ coefficient is then obtained via a Sommerfeld expansion of the free energy and of the energy potentials of the rapidities. After tedious algebra we obtain that the contribution of each band of rapidities is inversely proportional to the corresponding group velocity,

$$\gamma/N_a = (\pi/3)\left[\frac{1}{v_F} + \frac{1}{v_{cf}} + \frac{1}{v_{sw}^{(1)}} + \frac{1}{v_{sw}^{(3)}}\right]. \tag{5.1}$$

Here the term involving v_F is present in the metallic phase, but not in the insulating one. The zero-magnetic-field γ as a function of n_e for $N_e = N_a$ and several U values is shown in figure 7(A). γ increases monotonically with U and diverges as $U \to \infty$ since v_{cf} and $v_{sw}^{(l)}$ tend to zero. In that limit an infinitesimal H (or Δ) aligns all spins (empties the excited-electron band) and the specific heat is not proportional to T. On the other hand, γ monotonically decreases with increasing n_e and diverges as $n_e \to 0$ as a consequence of the van Hove singularity of the empty excited-electron band. For $n_e = 0.5$ the electron bands are degenerate ($\Delta = 0$) and we recover the result for the SU(4)-invariant case.

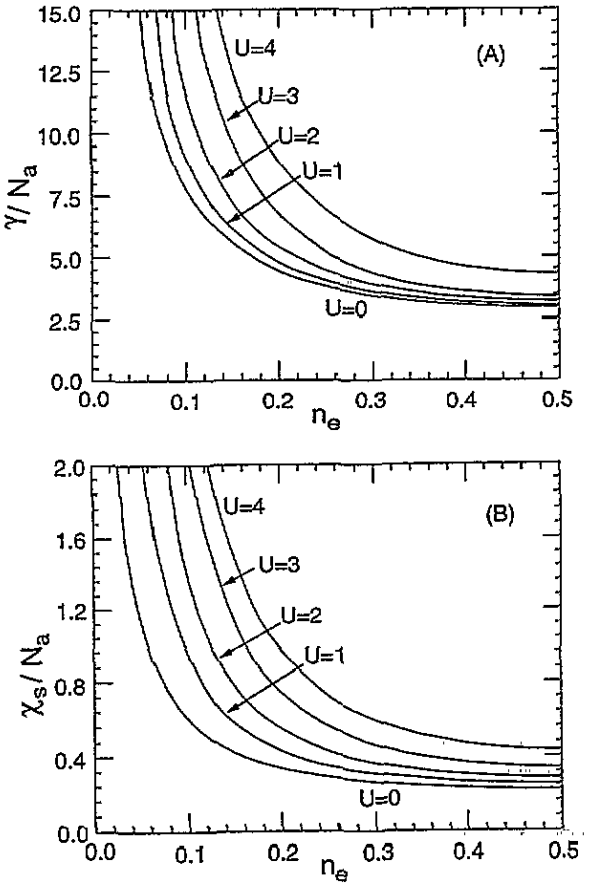

Figure 7. (A) Specific-heat coefficient γ and (B) magnetic susceptibility χ_S as a function of n_e for $n = 1$ and several U. Both are decreasing functions of n_e and increase with increasing U. Both quantities diverge as $U \to \infty$, since the spin waves and the crystalline-field excitations become soft in this limit. For $n_e \to 0$ the quantities diverge as a consequence of the van Hove singularity of the empty excited electron band.

The susceptibility can be obtained as the linear response to a magnetic field. Since there are two electron bands that can be polarized, there are two contributions to the susceptibility, $\chi_S = \chi^{(1)} + \chi^{(3)}$. If the field is small B_1 and B_3 are large and we can expand equations (2.3*b*), (2.3*d*), (2.7*b*) and (2.7*d*) for large $|\xi|$, i.e. for $|\xi| \gg B, Q$. The ξ dependence of the driving terms is then exponential, proportional to $\exp(-2\pi|\xi|/U)$, for all four equations. Since the integration kernels of the integral equations are the same, the magnetizations of the two bands are both proportional to H. To establish the relation of B_1 and B_3 with H we write (2.7*b*) and (2.7*d*) as a sequence of Wiener–Hopf integral equations. After a standard but tedious calculation we obtain that

$$\chi^{(1)} v_{sw}^{(1)} = \chi^{(3)} v_{sw}^{(3)} = \frac{1}{2\pi} \tag{5.2}$$

where $v_{sw}^{(l)}$ is given by (4.10). This relation holds for all U and n_e. Since the spin-wave velocities vanish as $U \to \infty$, the susceptibility diverges in that limit.

The susceptibility for $n = 1$ and several U is displayed in figure 7(B) as a function of n_e. χ_S and γ have a similar dependence on U and n_e. χ_S increases with increasing U and decreases with increasing n_e. It diverges as $n_e \to 0$ due to the van Hove singularity of the empty excited-electron band. The limit $n_e = 0.5$ does, however, not correspond to the SU(4) situation, since within our model the Zeeman field does not couple to an effective spin $\frac{3}{2}$ but to two spins $\frac{1}{2}$.

If the field is small but non-zero, logarithmic singularities appear in the susceptibility, caused by the interference between the two Fermi surface points of the spin-rapidity bands,

$$\chi_S(H)/\chi_S(0) = \left[1 + 1/\mathrm{Ln} - \ln(\mathrm{Ln})/\mathrm{Ln}^2 + \ldots\right] \tag{5.3}$$

where $\mathrm{Ln} = 2|\ln(H)|$ [12, 24].

6. Concluding remarks

We have considered a system consisting of two one-dimensional tight-binding bands with a Hubbard-like interaction, which can be reduced to the SU(4) generalization of Lieb and Wu's [10] Bethe *ansatz* solution of the traditional spin-$\frac{1}{2}$ Hubbard model. We have presented a detailed study of the ground-state properties, the spectrum of elemental excitations, the low-T specific heat and the magnetic susceptibility. The motivation for the study is twofold: (a) to obtain a better understanding of the metal–insulator transition the system undergoes for exactly one electron per site and (b) some experimental evidence for the participation of the $3d_{z^2}$ orbitals of Cu (besides the dominant $3d_{x^2-y^2}$ orbitals) in the properties of CuO-based high-temperature superconductors.

The model is integrable by construction. The two bands have equal dispersion and are split by a crystalline field Δ. For $\Delta = 0$ the system reduces to the SU(4)-invariant generalization of the Hubbard model, which for one electron per site has a Mott transition at $U_c = 2.981$. On the other hand, for Δ larger than a critical value $\tilde{\Delta}$,

$$\tilde{\Delta} = -\int_{-Q}^{Q} \mathrm{d}k \cos(k)\ G_1(\sin k)\ \epsilon(k) \tag{6.1}$$

the upper electron band is empty and the model is just the traditional spin-$\frac{1}{2}$ Hubbard model, which for $n = 1$ is an insulator for all repulsive U ($U_c = 0$). As the population of the

excited-electron band, n_e, is increased from 0 to 0.5 the critical interaction strength that localizes the charges, U_c, interpolates between the values 0 and 2.981. For small n_e this dependence is non-analytic, $n_e \approx U_c^{1/2}\exp(-2\pi/U_c)$.

The metallic and insulating phases are best characterized by the Fermi velocity of the charges. For the metal v_F is finite, while in the case of an insulator the Fermi velocity is zero. If $n < 1$ the system is always a metal. As the Mott transition is approached from the metallic phase (for $n = 1$), the Fermi velocity diverges, as a consequence of the vanishing of the density of charges at the Fermi level, $\rho(Q)$. This property has been used to determine the phase boundary between the metal and the insulator. For the insulator the range for the charge rapidities is the interval $[\pi, -\pi]$, while for the metal $Q < \pi$.

We studied the ground-state energy, the chemical potential and the crystalline-field splitting between the electron bands for one electron per site as a function of n_e and U. In these quantities the metal–insulator transition is only markedly seen as a discontinuity in the slope of μ with n_e. This is expected since μ is the energy necessary to remove an electron from the system, which should have a different dependence in the metal than in the insulator. This discontinuity is much weaker in the slope of Δ.

The spectrum of elemental excitations consists of four branches, one branch of charge excitations, one set of crystalline-field excitations and two branches of spin waves. The elemental excitations are soliton-like, i.e., the superposition principle holds and actual excitations can be built up as linear combinations of elemental ones. Hence, actual excitations then acquire a continuous energy spectrum for a given momentum. For $n = 1$ we only have 'hole'-like charge excitations. The most dramatic difference between the metal and the insulator is the Fermi velocity as discussed above. The crystalline field excitations have a Fermi surface (the excitation energy vanishes) with Fermi momentum $p_{cfF} = \pi n_e$, and hence the branch has 'particle'- and 'hole'-like excitations. The most important characteristics in this dispersion besides the Fermi momentum is the corresponding group velocity, v_{cf}, which is considerably affected by the metal–insulator transition. The momentum range of the spin waves is also determined by the number of electrons in each of the bands. In the absence of a magnetic field, there are only 'hole'-like spin-wave excitations. The spin-wave velocities of the two bands increase with the number of electrons occupying the respective band, and decrease with U. For $U \to \infty$ the crystalline field and both spin-wave branches become soft, as a consequence of the excluded multiple occupancy of each site.

The magnetic susceptibility and the linear-T coefficient of the specific heat, γ, are both determined by the group velocities of the branches of elemental excitations. Both are increasing functions of U and diverge as $U \to \infty$. They also diverge as $n_e \to 0$ as a consequence of the van Hove singularity of the empty excited electron band.

Acknowledgment

The support of the Department of Energy under grant DE-FG05-91ER45443 is acknowledged.

Appendix. The $U = 0$ solution

In the $U \to 0$ limit and zero magnetic field the solution of (2.3) for the rapidity distribution densities is

$$\rho(k) = \begin{cases} 2/\pi & \text{if } |k| \leqslant \sin^{-1}(B) \\ 1/\pi & \text{if } \sin^{-1}(B) < |k| \leqslant Q \\ 0 & \text{elsewhere} \end{cases} \tag{A.1}$$

$$\sigma_2(\Lambda) = \begin{cases} 1/[\pi\sqrt{1-\Lambda^2}] & \text{if } |\Lambda| \leqslant B \\ 0 & \text{elsewhere} \end{cases} \tag{A.2}$$

$$\sigma_1(\xi) = \tfrac{1}{2}\left[\sigma_2(\xi) + \rho(\sin^{-1}(\xi)) \,/\, \sqrt{1-\xi^2}\right] \tag{A.3}$$

$$\sigma_3(\xi) = \tfrac{1}{2}\sigma_2(\xi). \tag{A.4}$$

For a band occupation of exactly one electron per site, $n = N_e/N_a = 1$, the integration limits B and Q are not independent, but related via

$$Q + \sin^{-1}(B) = \pi/2\ . \tag{A.5}$$

The populations of the bands are

$$n_e = \int_{-B}^{B} d\Lambda\ \sigma_2(\Lambda) = \frac{2}{\pi}\sin^{-1}(B) \qquad n_g = 1 - n_e \tag{A.6}$$

and the energy is given by

$$E/N_a = \int_{-Q}^{Q} dk\ [-2\cos(k)]\ \rho(k) = -\frac{4}{\pi}[B + \sin(Q)]. \tag{A.7}$$

The energy potentials are obtained in a similar way (zero magnetic field)

$$\epsilon(k) = \begin{cases} -8\cos(k) - 4\mu + 2\Delta & \text{if } |\sin(k)| \leqslant B \\ -4\cos(k) - 2\mu & \text{if } B < |\sin(k)| \leqslant \sin(Q) \\ -2\cos(k) - \mu & \text{elsewhere} \end{cases} \tag{A.8}$$

$$\varphi^{(2)}(\Lambda) = \begin{cases} 2\Delta - 2\mu - 4\sqrt{1-\Lambda^2} & \text{if } |\Lambda| \leqslant B \\ \Delta - \mu - 2\sqrt{(1-\Lambda^2)} & \text{if } B < |\Lambda| \leqslant \sin(Q) \\ \Delta & \text{elsewhere} \end{cases} \tag{A.9}$$

$$\varphi^{(1)}(\xi) = \begin{cases} \dfrac{1}{2}\left[\varphi^{(2)}(\xi) + \rho(\sin^{-1}(\xi))\right] & \text{if } |\xi| \leqslant B \\ \dfrac{1}{2}\rho(\sin^{-1}(\xi)) & \text{if } B < |\xi| \leqslant \sin(Q) \\ 0 & \text{elsewhere} \end{cases} \tag{A.10}$$

$$\varphi^{(3)}(\xi) = \begin{cases} \dfrac{1}{2}\varphi^{(2)}(\xi) & \text{if } |\xi| \leqslant B \\ 0 & \text{elsewhere.} \end{cases} \tag{A.11}$$

The chemical potential, μ, and the band splitting, Δ, are determined from $\epsilon(\pm Q) = 0$ and $\varphi^{(2)}(\pm B) = 0$ $(n = 1)$

$$\mu = -2\cos(Q) \qquad \Delta = 2\sin(Q) - 2\cos(Q). \tag{A.12}$$

References

[1] Anderson P W 1987 *Science* **235** 1196; 1990 *Phys. Rev. Lett.* **64** 1839
[2] Komskii D I 1971 *Physica* B **171** 44
[3] Takagi H, Tokura Y and Uchida S 1989 *Mechanisms of High Temperature Superconductivity (Springer Series in Material Science XX)* ed H Kamimura and A Ochiyama (Berlin: Springer) p 238
[4] Bianconi A, Castrucci P, Fabrizi A, Pompa M, Flank A M, Lagarde P, Katayama-Yoshida H, Kotani A and Marcelli A 1988 *Phys. Rev.* B **38** 7196
Bianconi A, Castrucci P, Fabrizi A, Pompa M, Flank A M, Lagarde P, Katayama-Yoshida H and Calestani G 1989 *Physica* C **162–164** 209; 1990 *Earlier and Recent Aspects of Superconductivity* ed J G Bednorz and K A Müller (Berlin: Springer) p 407
[5] Nucker A, Romberg H, Xi X X, Fink J, Gegenheimer B and Zhao Z X 1989 *Phys. Rev.* B **39** 6619
[6] Bianconi A 1990 *Proc. Int. Conf. on Superconductivity* ed S K Joshi, C N R Rao and S V Subramanyam (Singapore: World Scientific) p 448
[7] Balseiro C A, Avignon M, Rojo A G and Alascio B 1989 *Phys. Rev. Lett.* **62** 2626
Muttalib K A and Emery V J 1986 *Phys. Rev. Lett.* **57** 1370
Aoki H and Kuroki K 1990 *Phys. Rev.* B **42** 2125;
Buda F, Cox D L and Jarrell M 1994 *Phys. Rev.* B **49** 1255
[8] Schlottmann P 1992 *Phys. Rev. Lett.* **68** 1916; 1994 *J. Appl. Phys.* **75** 6731; 1994 *Phys. Rev.* B **49** 6132
[9] Schlottmann P 1992 *Phys. Rev. Lett.* **69** 2396; 1993 *J. Appl. Phys.* **73** 6645
[10] Lieb E H and Wu F Y 1969 *Phys. Rev. Lett.* **20** 1445
[11] Choy T C 1980 *Phys. Lett.* **80A** 49
Haldane F D M 1980 *Phys. Lett.* **80A** 281
Choy T C and Haldane F D M 1982 *Phys. Lett.* **90A** 83
[12] Lee K and Schlottmann P 1989 *Phys. Rev. Lett.* **63** 2299
[13] Schlottmann P 1991 *Phys. Rev.* B **43** 3101
[14] Schlottmann P 1992 *Phys. Rev.* B **45** 5784
[15] Lee K and Schlottmann P 1990 *Physica* B **163** 398
[16] Lee K and Schlottmann P 1989 *J. Phys.: Condens. Matter* **1** 10193
[17] Sutherland B 1975 *Phys. Rev.* B **12** 3795
[18] Sutherland B 1978 *Rocky Mount. J. Math.* **8** 413
[19] Frahm H and Schadschneider A 1993 *J. Phys. A: Math. Gen.* **26** 1463
[20] Sutherland B 1968 *Phys. Rev. Lett.* **20** 98
[21] Coll C F III 1974 *Phys. Rev.* B **9** 2150
[22] Ovchinnikov A A 1969 *Zh. Eksp. Teor. Fiz.* **57** 2137 (Engl. Transl. 1970 *Sov. Phys.–JETP* **30** 1160)
[23] Takahashi M 1972 *Prog. Theor. Phys.* **47** 69
[24] Schlottmann P 1991 *Physical Phenomena at High Magnetic Fields* ed E Manousakis, P Schlottmann, P Kumar, K S Bedell and F M Mueller (Reading MA: Addison-Wesley) p 502